Interpreter input for seismic image segmentation

Adam Halpert

ABSTRACT

While automatic segmentation of seismic images can dramatically speed up interpretation of salt bodies and alleviate a major model-building bottleneck, human expertise at this task is valuable and should be included. Here, I demonstrate a strategy to incorporate such expertise into the highly-efficient Pairwise Region Comparison (PRC) segmentation algorithm. By supplying a limited manual interpretation of the salt boundary, interpreters can correct local inaccuracies and guide the automatic result in both two and three dimensions. In the 3D case, accuracy of the segmentation improves even in areas far from the manual picks. Examples from a wide-azimuth Gulf of Mexico survey demonstrate the effectiveness of this procedure.

INTRODUCTION

Automated seismic image segmentation allows for fast interpretation of regions within seismic images, and is especially useful for identifying large subsurface salt bodies that are tedious to interpret manually. This automation helps to alleviate a substantial bottleneck within the iterative imaging, interpretation and model-building workflow. At this point, however, complete automation is not a feasible or even desirable goal. Experienced human interpreters offer a great deal of expertise, especially in complex geological settings where computers are unable to provide an accurate automatic interpretation. Here, I discuss a strategy for incorporating such expertise into the framework of automated image segmentation.

Beyond relatively simple horizon auto-picking, which tends to get lost along chaotic or discontinuous boundaries, a variety of options exist for *global* image segmentation. One useful approach, developed by Lomask et al. (2007), uses the eigenvector-based Normalized Cuts Image Segmentation (NCIS) method (Shi and Malik, 2000). However, this method is relatively inefficient; large seismic images require substantial preprocessing, and the computational domain must be windowed around a prior best-guess of the boundary to make the method computationally feasible. More recent work (Halpert et al., 2010) adopts a "Pairwise Region Comparison" (PRC) approach based on the method of Felzenszwalb and Huttenlocher (2004). This method holds several advantages over the NCIS approach, including computational efficiency and the ability to operate on full seismic images. In this paper, the PRC method is used as a basis to explore how an interpreter's own top- or base-salt picks can influence

automated segmentation results in two or three dimensions. Throughout the paper, I show 2D (Figure 1(a)) and 3D (Figure 1(b)) field data examples from a wide-azimuth Gulf of Mexico dataset provided by WesternGeco.

SEGMENTATION METHOD

The PRC segmentation algorithm is a graph-based method that relies heavily on the concept of "minimum spanning trees" (Zahn, 1971). In short, the algorithm makes comparisons between pairs of nearby pixels in a migrated image, and determines whether the pixels belong in the same image segment, or in separate regions. See Halpert (2010) for full details on how this method is adapted for seismic images. This algorithm is very efficient compared to other segmentation techniques such as NCIS; for example, the 1000 x 1000 pixel 2D result here was computed in less than a minute, while the 3D result (1000 x 800 x 40) required 10 minutes on a single processor. Parallelization of this scheme is made possible by operating simultaneously on different chunks of the input cube, although additional pre- and post-processing is necessary. Segmentation results (for example, Figures 2(a) or 5(a)) are shown as random-color segments overlying the image. Very few parameters are required; the user controls the minimum segment size, and can quickly choose segments to merge together in two or three dimensions. All results shown here required merging 5-10 segments within the salt body.

INTERPRETER GUIDANCE

It is clear from the initial 2D segmentation result in Figure 2(a) that the algorithm did not perform ideally in several locations. Specifically, the salt segment "leaks" through the boundary at two locations, one along the top of the salt body and one along the base. In such situations, we want to use interpreter input to rectify the inaccuracies. Figure 2(b) shows manual interpretations of the salt boundary in the region where the leakages occurred. These boundary segments were quickly picked using a few seed points and an auto-picker.

At this point, these manual interpretations must somehow be incorporated into the automated framework of the PRC method. Broadly speaking, this can be done in two ways. First, we can modify the algorithm itself to check for the manual interpretations when assigning weights to pixel pairs. However, this option adds unnecessary complexity to the process and would likely severely curtail the algorithm's efficiency (one of its major advantages). Alternatively, we could modify the input data according to the picks, and allow the segmentation algorithm to proceed normally. Since this option preserves the algorithm's efficient structure, I focus here on modifying the input amplitude of the envelope volumes to accommodate the manual interpretations.

A simple solution to the problem would involve assigning a high amplitude value to the manually picked points. While this is the basic idea behind the solution described

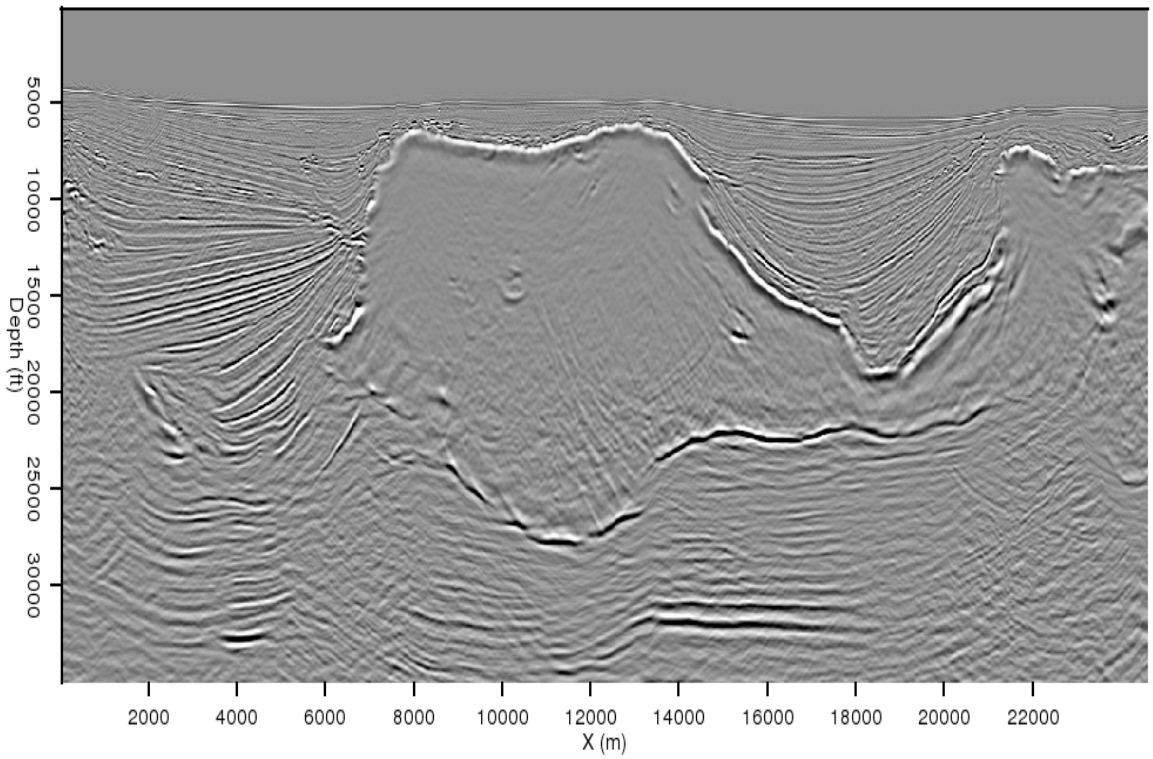

(a)

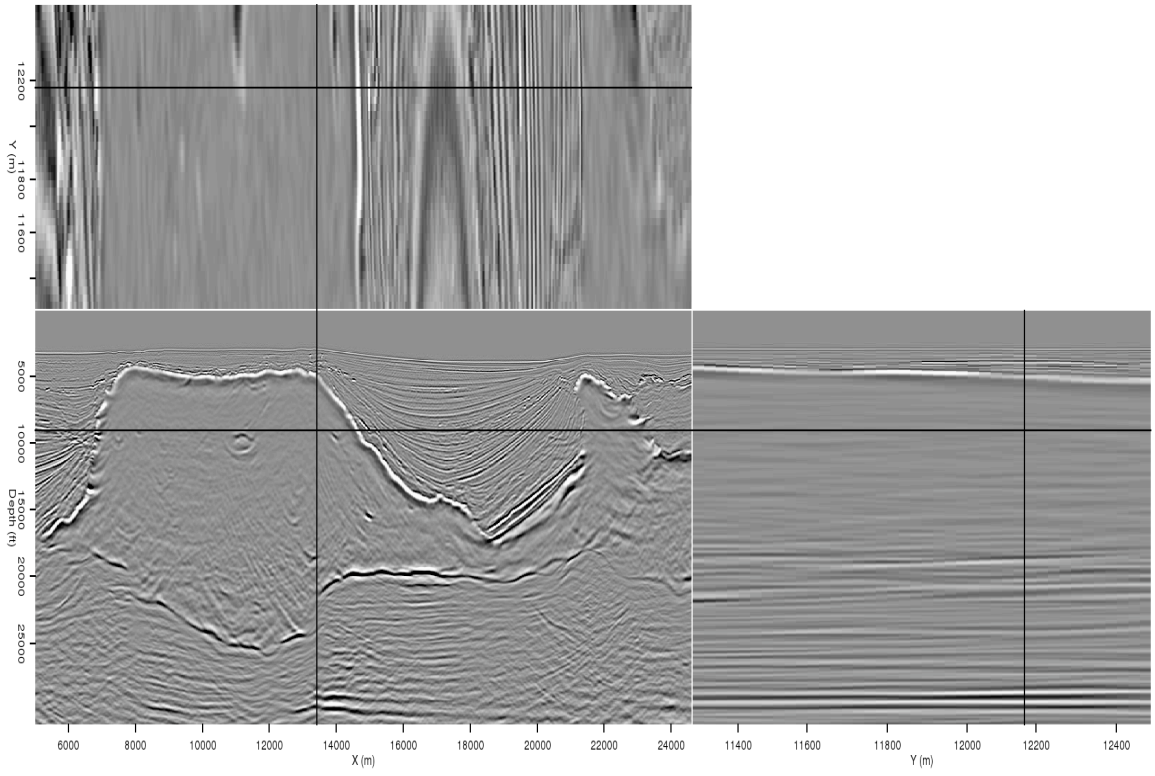

(b)

Figure 1: (a) 2D and (b) 3D images taken from a field dataset that will be used for examples throughout this paper. [**ER**]

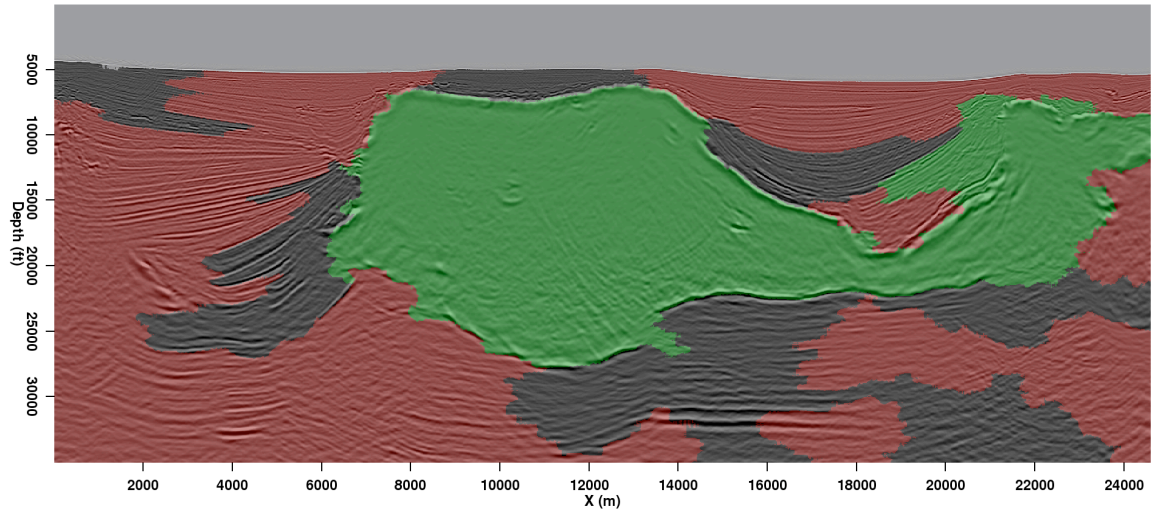

(a)

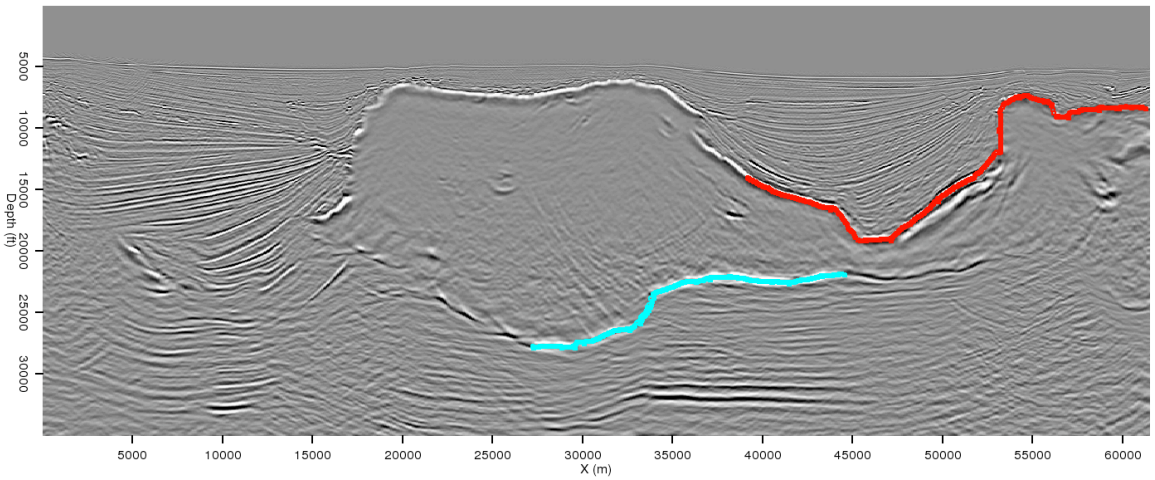

(b)

Figure 2: (a) 2D segmentation result without interpreter guidance. The salt body segment shows significant "leakage" at the locations indicated. (b) Manual interpretations of the salt boundary near where the leakages occurred. [**ER**]

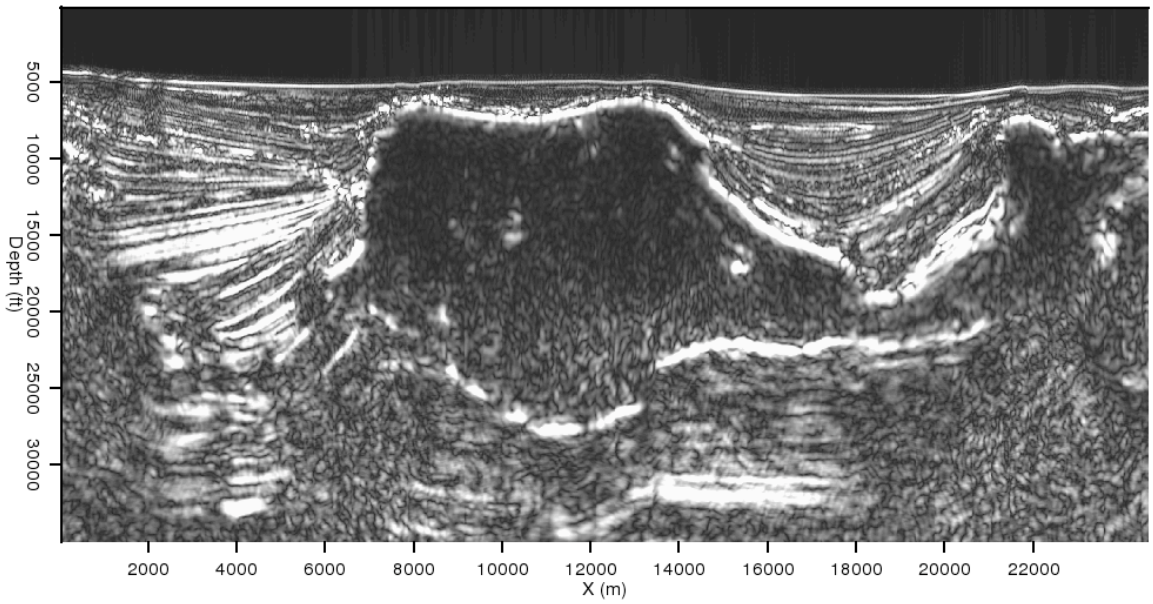

(a)

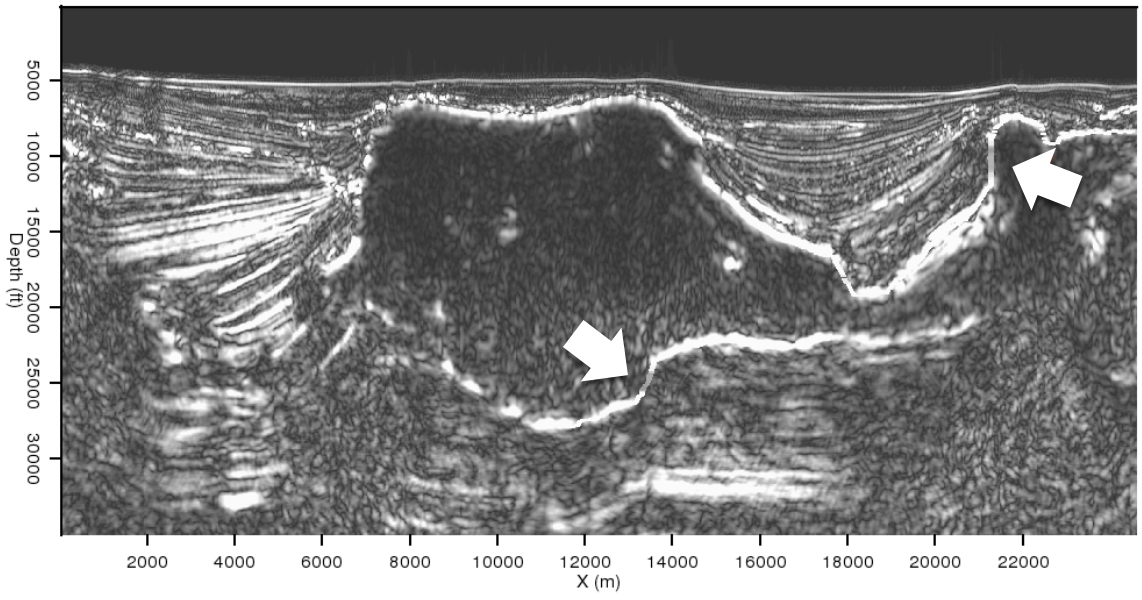

(b)

Figure 3: Amplitude of the envelope calculations from the original image (a), and modified according to the manual salt picks in Figure 2(b). The salt boundary is clearer and more continuous in the modified image, especially at the indicated locations. [**ER**]

here, it is unfortunately not quite so straightforward. Assigning high amplitudes to a string of points without regard to neighboring amplitude values causes the algorithm to treat the manual interpretation as a segment distinct from those surrounding it, even those also inside a salt body. Instead, I define a new amplitude value (A) for a "picked" pixel at position (x,y,z) in terms of the highest-amplitude pixel in a neighborhood surrounding it and a scaling factor α:

$$A_{xyz} = \alpha \max_{ijk} A_{ijk}, \tag{1}$$

where i, j, and k are constrained by $|x-i| \leq 5, |y-j| \leq 5, |z-k| \leq 5$. This approach ensures that a boundary will be emphasized on the input data where it has been manually picked, but will not appear radically different from its surroundings. Figures 3(a) and 3(b) illustrate this idea; the manually picked points are now clearly visible in panel (b), but the character of the boundary does not change noticeably. Now, segmenting the new input image with parameters identical to the original segmentation yields the result seen in Figure 4. The segments conform to the manual picks seen in Figure 2(b), while the rest of the image is segmented as accurately as the original result in Figure 2(a).

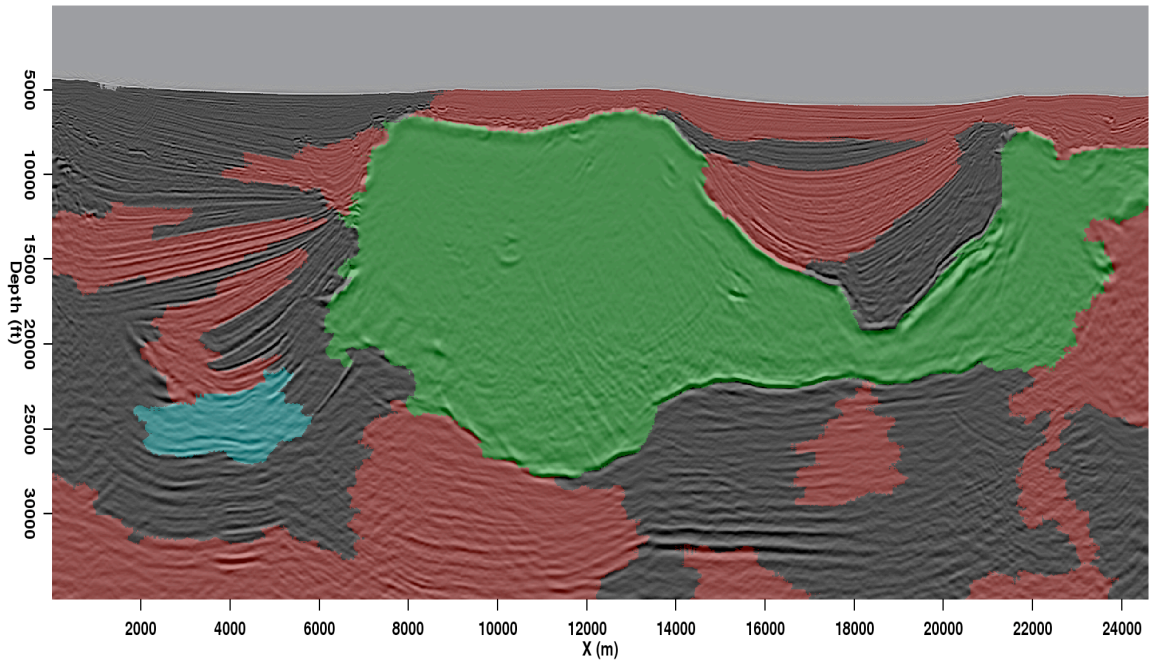

Figure 4: 2D interpreter-guided segmentation results. This result incorporates the manual picks seen in Figure 2(b). [**ER**]

THREE DIMENSIONS

While the PRC algorithm suffers from the same leakage problem in 3D (Figure 5(a)) seen in the 2D example, the same solution cannot be applied. Because segments are

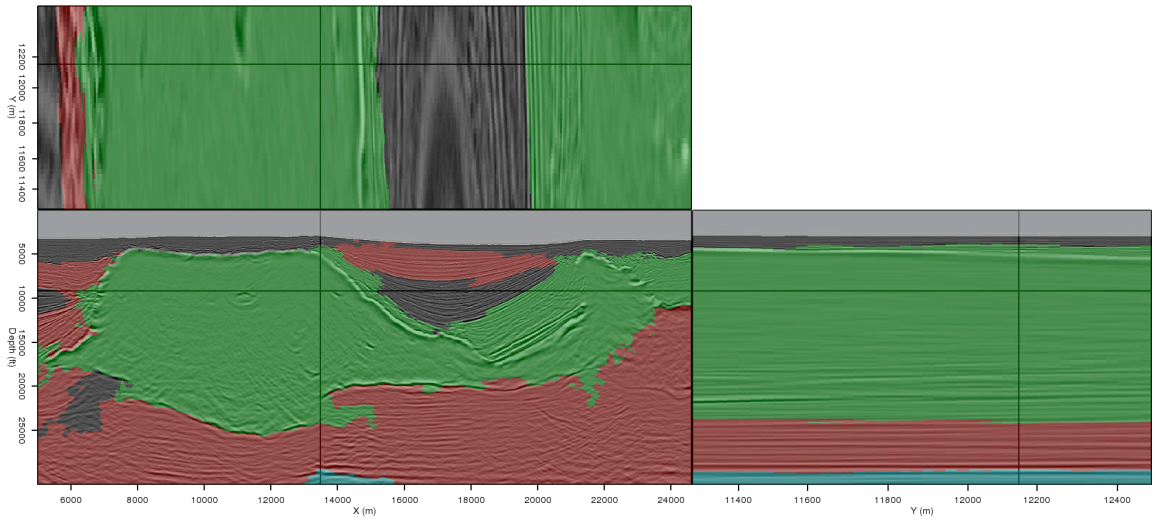

(a)

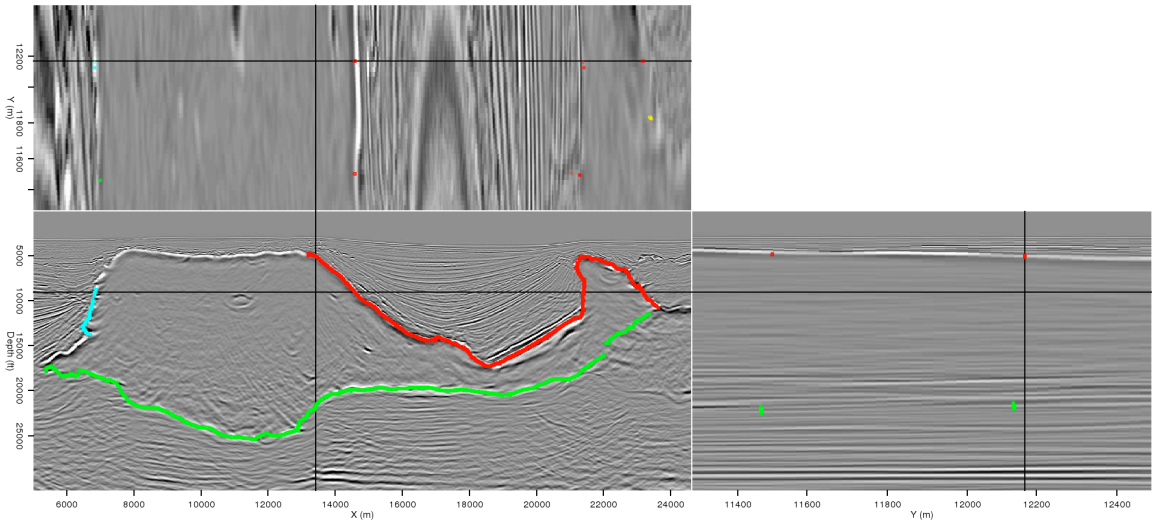

(b)

Figure 5: (a) 3D segmentation result prior to any interpreter guidance. (b) Manually interpreted salt boundary picks. Manual picks from one or more sections are used to guide the automatic 3D segmentation. [**ER**]

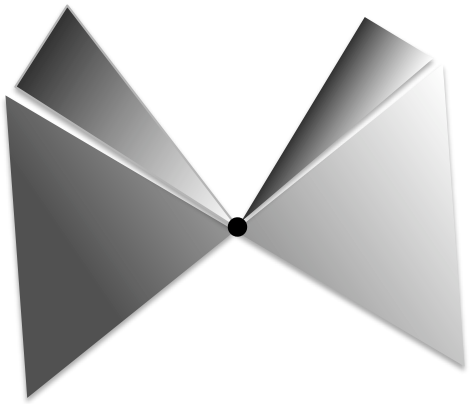

Figure 6: Schematic illustrating the concept of "spraying" manual interpretations of a 2D section into the third dimension. The black dot represents a pixel along a manually-picked horizon. [**NR**]

much larger in 3D, amplitude changes on a single 2D section are not significant enough to alter 3D segmentation results. Instead, we must "project" an interpreter's manual picks on an inline section, like those seen in Figure 5(b), into the third (crossline) dimension. If we make the assumption that the dip of the salt flank does not fluctuate by more than two pixels per slice in the crossline direction, we can construct a square pyramid (Figure 6) in the crossline direction with sides of length $2h$, where h is the number of crossline samples between the base of the pyramid and its apex, which is the manually interpreted point P. Now, the new amplitude value for any pixel Q that falls within the pyramid is

$$A^Q_{\text{new}} = A^Q_{\text{orig}} + \frac{A_0}{||PQ||}, \tag{2}$$

where A_0 is the amplitude value at point P as determined by equation (1), and $||PQ||$ is the distance between the two points. As seen in Figure 7(b), the interpreter's picks now influence amplitude values in all three directions, but the magnitude of that influence decays with distance from the manual picks. Accordingly, the updated 3D segmentation result in Figure 8 is improved throughout the image cube, and not just on the two inline sections where manual picks were provided. For example, Figure 9 shows image slices far away from the two crosslines for which manual interpretations were supplied. In Figures 10(a) and 10(b), the effects of the 3D interpreter input procedure on the envelope volumes are apparent. Figures 11(a) and 11(b) compare the original and interpreter-guided segmentation results for this location, demonstrating that the 3D segmentation results can improve dramatically even far away from any manual pick locations.

CONCLUSIONS

The Pairwise Region Comparison algorithm offers a highly efficient means of automatically segmenting salt bodies in seismic images, but its accuracy can suffer in areas with discontinuous boundaries or poor illumination. In such cases, altering the input amplitude data according an interpreter's manual picks can successfully guide

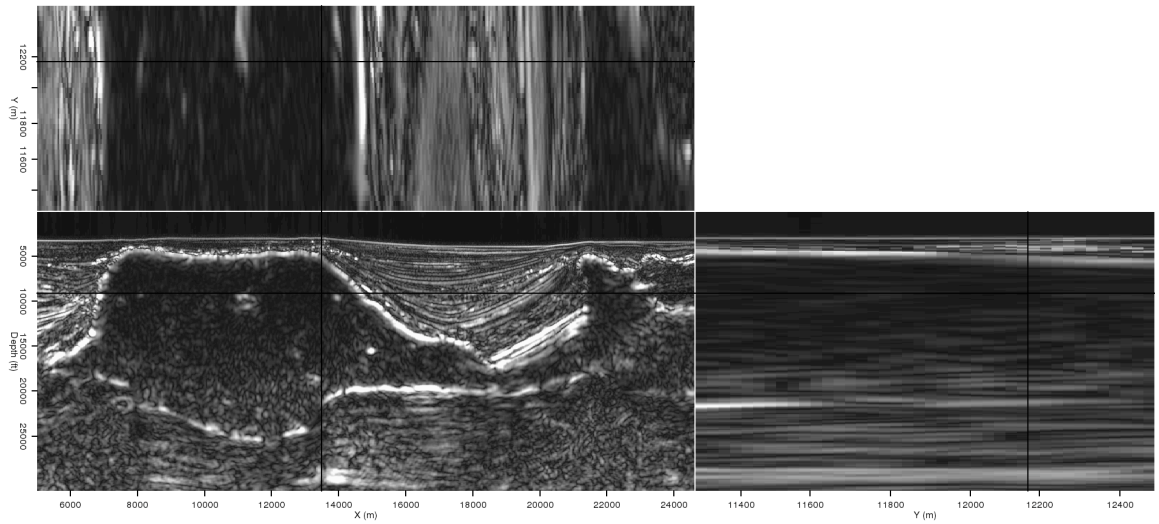

(a)

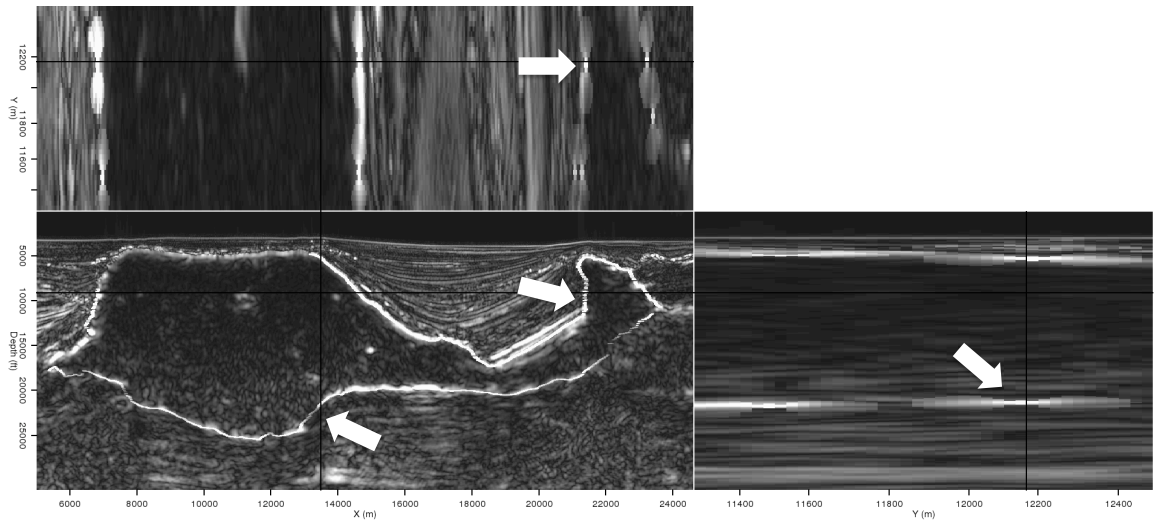

(b)

Figure 7: 3D amplitude of the envelope calculations from (a)the original image, and (b) modified according to the manual picks seen in Figure 5(b). The 3D effects of the procedure to incorporate the picks are evident on the crossline and depth slices. [**ER**]

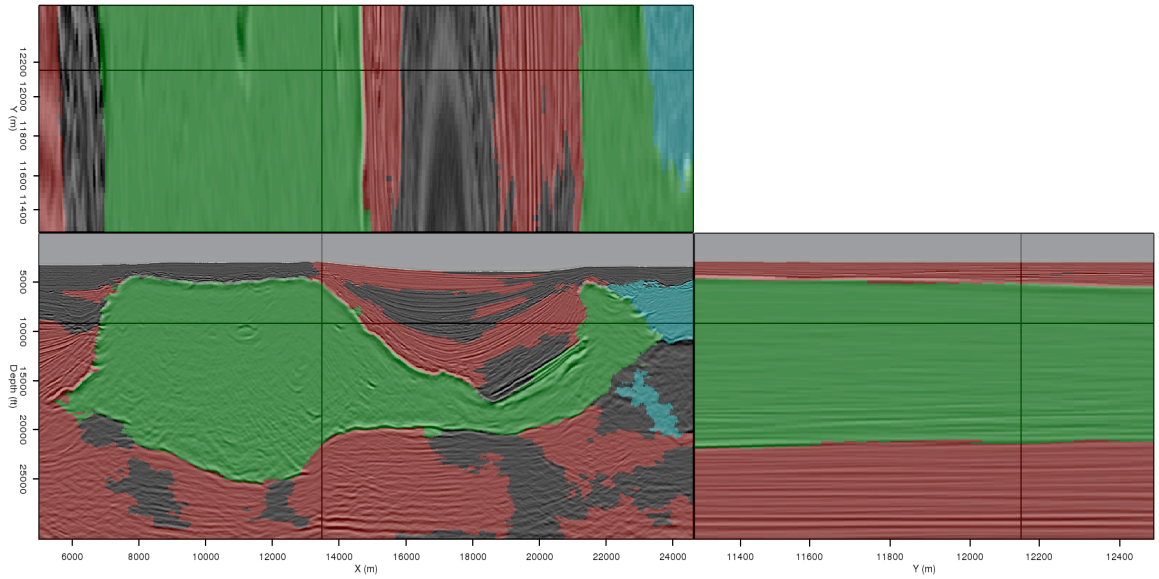

Figure 8: 3D interpreter-guided segmentation results, incorporating the picks seen in Figure 5(b). Note that in this result, the segmentation is more accurate in all three directions. [**ER**]

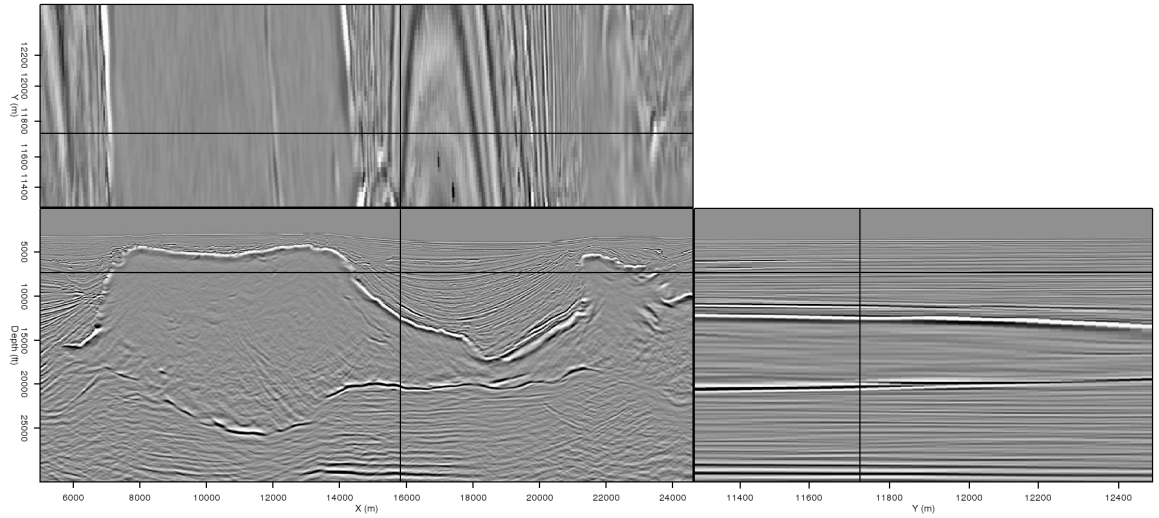

Figure 9: Slices from the 3D image cube far away from any interpreter-supplied salt picks. [**ER**]

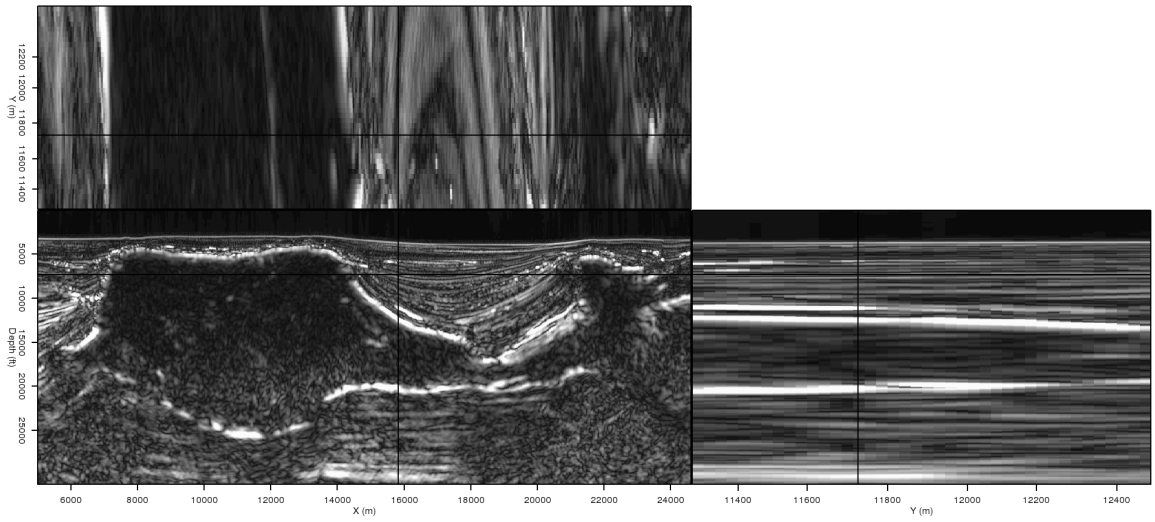

(a)

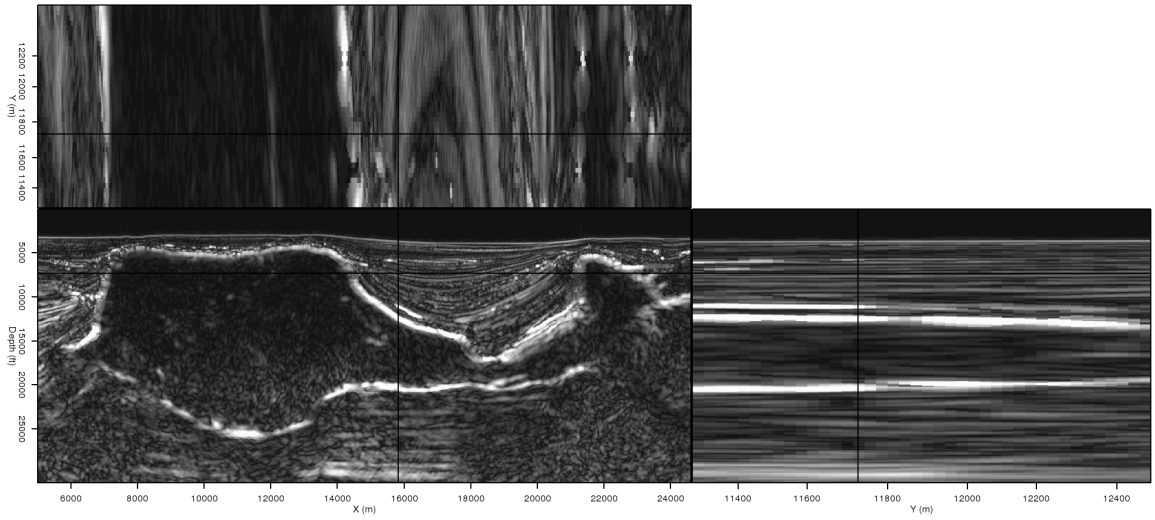

(b)

Figure 10: Envelope volumes at the position of the image slices seen in Figure 9, (a) before and (b) after incorporating interpreter input from a distant location. In (b), continuity of the salt boundary is improved, allowing a more accurate segmentation result. [**ER**]

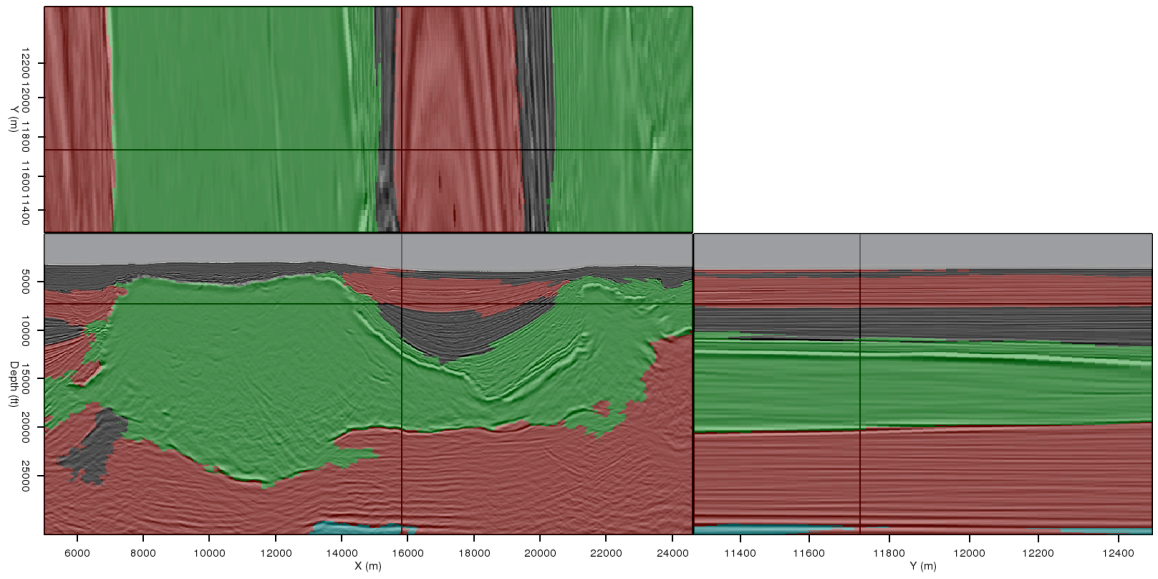

(a)

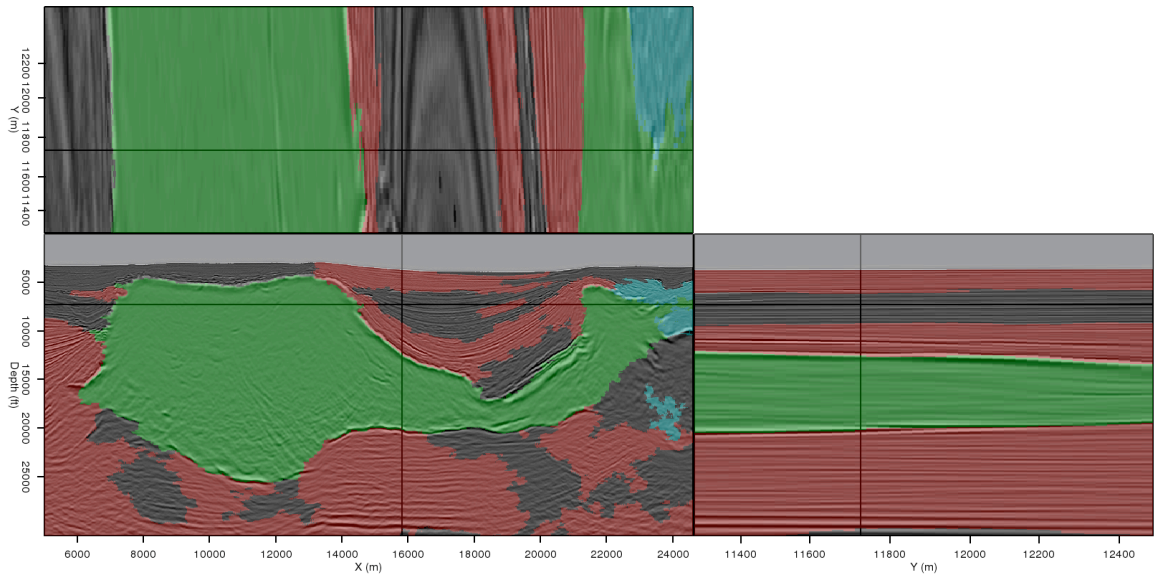

(b)

Figure 11: A comparison of segmentation results (a) without using interpreter input, and (b) after incorporating information from the picks in Figure 5(b). Even though the data slices shown here are far from the location of the manual picks, the strategy of spreading information from 2D picks into the third dimension allows for a much more accurate result in (b). [**ER**]

the segmentation to a more accurate result, even in areas far from the manual picking locations. Combining interpreter expertise with automation in this manner could help alleviate a major bottleneck in the model-building and imaging workflow.

ACKNOWLEDGMENTS

I thank WesternGeco for providing the field dataset used for examples, and all sponsors of the Stanford Exploration Project for their support.

REFERENCES

Felzenszwalb, P. F. and D. P. Huttenlocher, 2004, Efficient graph-based image segmentation: International Journal of Computer Vision, **59**, 167–181.

Halpert, A., 2010, A new method for more efficient seismic image segmentation: SEP-Report, **140**, 213–228.

Halpert, A., R. G. Clapp, and B. L. Biondi, 2010, Speeding up seismic image segmentation: SEG Technical Program Expanded Abstracts, **29**, 1276–1280.

Lomask, J., R. G. Clapp, and B. Biondi, 2007, Application of image segmentation to tracking 3d salt boundaries: Geophysics, **72**, P47–P56.

Shi, J. and J. Malik, 2000, Normalized cuts and image segmentation: Institute of Electrical and Electronics Engineers Transactions on Pattern Analysis and Machine Intelligence, **22**, 838–905.

Zahn, C. T., 1971, Graph-theoretical methods for detecting and describing gestalt clusters: IEEE Transactions on Computers, **C-20**, 68–86.